A Control Algorithm for Electric Vehicle Fast Charging Stations Equipped with Flywheel Energy Storage Systems

Sun, Bo; Dragicevic, Tomislav; Freijedo Fernandez, Francisco Daniel; Quintero, Juan Carlos Vasquez; Guerrero, Josep M.

Published in:
I E E E Transactions on Power Electronics

DOI (link to publication from Publisher):
10.1109/TPEL.2015.2500962

Publication date:
2016

A Control Algorithm for Electric Vehicle Fast Charging Stations Equipped with Flywheel Energy Storage Systems

Bo Sun, *Student Member, IEEE*, Tomislav Dragiˇcevi´c, *Member, IEEE*, Francisco D. Freijedo, *Member, IEEE,* Juan C. Vasquez, *Senior Member, IEEE*,
Josep M. Guerrero, *Fellow, IEEE*
www.microgrids.et.aau.dk

***Abstract*—This paper proposes a control strategy for plug-in electric vehicle (PEV) fast charging station (FCS) equipped with a flywheel energy storage system (FESS). The main role of the FESS is not to compromise the predefined charging profile of PEV battery during the provision of a hysteresis-type active power ancillary service to the overhead power system. In that sense, when the active power is not being extracted from the grid, FESS provides the power required to sustain the continuous charging process of PEV battery. A key characteristic of the whole control system is that it is able to work without any digital communication between the grid-tied and FESS converters. Detailed system modeling and dynamics analysis of the controller are carried out for the different operating modes of the FCS system. A lab-scale prototype was built to validate the proposal. The presented experimental results proved the high accuracy of the theoretical analysis.**

***Index Terms*—Flywheels, fast charging stations (FCS), distributed control, plug-in electric vehicles (PEV)**

I. Introduction

NOWADAYS the increasing public awareness about environmental pollution and fossil fuels depletion is leading to dramatic expansion of renewable energy sources (RES), such as wind turbines and photovoltaics [1]–[3]. However, with the penetration of large amount of these variable sources, issues such as active power imbalance and frequency fluctuation are introduced in the operation of the power system [4]. It is therefore critical for system operators to set aside additional reserve capacities for ancillary services like frequency control and load following. Conventionally, this was provided by the generation units (supply side) [5]. Recently, the concepts of load control and demand response have been shifted into focus due to its potential to provide such services by aggregating large numbers of flexible loads into controllable entities. In such a manner, distributed system operators (DSO) could manage loads to support the overall grid stability and better optimize their power generation resources [6].

At the same time, transportation sector is changing towards a greater electrification of vehicle fleets. According to the Electric Power Research Institute, it is estimated that by 2020 the Europe's electric vehicle (EV) market is going to increase by 5 times, and up to 35% of the total vehicles in the U.S. will be plug-in EV (PEV) [7]. The industry has defined three levels of charging patterns for EVs [8]: Level 1 comprises an on-board single phase ac charger of up to $2\,\mathrm{kW}$ and usually takes place at residential households. Level 2 is typically used in private or public outlets with dedicated on-board single phase or three phase ac charger with power rating from $4\,\mathrm{kW}$ to $19.2\,\mathrm{kW}$. Level 3 has the highest power rating and uses a dedicated off-board dc charger of up to $240\,\mathrm{kW}$. This type of charger is often referred to as the fast charging station (FCS) [9].

The recommended charging profile is proprietary to the particular battery manufacturer, which commonly includes two stages: constant current and constant voltage stages. In [10] a typical Level 3 charging profile of Nissan leaf is given, the charging power is $50\,\mathrm{kVA}$ and duration time is around 30 minutes. Among the charging patterns, level 3 has the most significant impact on power system. FCSs will account for a considerable part of total energy consumption in future power systems and will have a great potential to provide flexible load control reserves managed by DSO [11]–[14].

Ancillary services by PEVs can be provided in different ways. For example, in [12] a vehicle to grid (V2G) based aggregation of PEVs is proposed to regulate the charging and discharging rate in order to contribute to the active power regulation of power system. In [13], PEV chargers are controlled in unidirectional way to simply switch on or off and modify the aggregated charging pattern. In [14], a hysteresis control originally used for thermostatically controlled loads [15] is employed for PEV charging to actively control the aggregated consumption of higher number of chargers. This is done by adapting individual PEV states of charge (SoC). The signals from upper-level controller are used to determine the instantaneous charging rate [14]. In order to keep the heath of battery, it is recommended that the charging profile defined by manufacturer is not interrupted [16]. However, the main limitation of all these strategies above is that the charging pattern recommended by battery manufacturers is compromised and thus the lifetime and reliability of PEV battery is reduced [16].

In order to mitigate the adverse effects of discontinuous charging of PEV batteries, type 3 FCS can be enhanced with local energy buffers based on energy storage system (ESS)

B. Sun, T. Dragičević, F. D. Freijedo, J. C. Vasquez, J. M. Guerrero are with the Department of Energy Technology, Aalborg University, 9220, Aalborg, Denmark. (Email: sbo@et.aau.dk; tdr@et.aau.dk; fran@et.aau.dk; juq@et.aau.dk; joz@et.aau.dk)

This paper was supported by ERANET EU Project Flex-ChEV, www.flexchev.et.aau.dk

[9], [10], [17]. Battery ESS (BESS) is one of the most extensively used ESS technologies in industrial applications [18], [19]. However degradation is still an unsolved problem for BESS [17], especially in the application considered in this paper, which is characterized by deep and frequent cycling. Compared with BESS, flywheel ESS (FESS) is a more suitable technology for providing frequent and fast power compensation services; it is a mature and economical technology, which has a high power density and virtually no degrading problems caused by frequent charging and discharging [9], [17]. This paper extends and provides experimental validation of the concept proposed in [9]: a lab scale prototype for a type 3 FCS with integrated FESS has been developed and experimental verification that proves its performance in different operation points has been carried out for the first time.

Regarding the design of flywheel, a standard induction machine may not be suitable for practical implementation if the flywheel is intended to operate at very high rotational speeds to maximize energy storage. Several specific constraints should be considered: low losses in standby mode to minimize self-discharging; run at rated power through wide range speed; good efficiency over all speed range; rotor losses and cooling condition. Practical design aspects of the flywheel are out of the scope of this paper. More details in this regard are given in [20]–[23].

FESS coupled to a common dc-link has been employed in the past [24]–[28]. In most cases, a centralized controller which relies on a high bandwidth communication among power converters is needed. Existence of communication links is a disadvantage, because it introduces a single point of failure and hence reduces the reliability of the system. In particular, breakdown of communication links will in general lead to a failure of the whole system. The implementation of distributed bus signaling (DBS) control overcomes this limitation [29]–[31]. DBS coordinates the grid and FESS converters by introducing droop based term in the FESS dc-link control loop. As shown in Section III, this key feature has been successfully implemented and experimentally tested here.

Based on the previous discussion, the contributions of this paper can be summarized as follows: 1) The DBS strategy has been appropriately modified for a type 3 FCS equipped with a FESS so as to support hysteresis type ancillary service, which permits to fulfill requirements of DSO and recommended PEV charging profiles at the same time. 2) The dynamic properties of this particular strategy have been comprehensively analyzed, and 3) Extensive experimental verification of the theoretical findings has been carried out.

The rest of the paper is organized as follows. Section II depicts the configuration of FCS and develops a dynamic model for individual components in the system. In Section III, a hysteresis control with integrated DBS method is proposed to achieve decentralized coordination between all units and the full scale control architecture used for theoretical assessment is presented. In Section IV, a detailed modeling of the system dynamics is provided. Experimental results that indicate the feasibility of proposed method are presented in Section V. Finally, Section VI gives the conclusion.

II. Configuration of the Fast Charging Station

Fig. 1 depicts the aggregation concept of a number of FCSs that resemble the structure originally proposed in [9]. The aggregators serving as intermediaries generate the control references to each individual local FCS by processing the DSO commands. The basic structure of each FCS system upgraded with a dedicated FESS is also detailed in Fig. 1: a set of PEV chargers and a pair of three-phase ac/dc converters are connected around the common dc bus with grid and FESS, respectively. A suitable control operation should fulfill DSO and PEV charging requirements at the same time, but also achieve a robust dc-link regulation (i.e., a stable and safe operation of the power electronics devices in all operating modes). The dc-link dynamics are set by the following equation:

$$C_{DC}\frac{dv_{DC}(t)}{dt} = i_{Gdc}(t) + i_{Fdc}(t) - i_{Ldc}(t) \tag{1}$$

where C_{DC} is the capacitance connected to the bus, $i_{Gdc}(t)$, $i_{Fdc}(t)$ and $i_{Ldc}(t)$ are the dc currents flowing from the grid and FESS, and extracted by the PEV charger(s) load, respectively. The PEV charger, grid and FESS converters have their own specific dynamic features, which are analyzed in the following sections.

A. Grid Interface

A two-level PWM rectifier is used to connect the FCS with the grid. A d-q synchronous reference frame is used for control. The dc-link voltage and reactive power controllers generate their corresponding current references. Assuming that the grid voltage is perfectly synchronized with the d-axis [$e_{Gd}(s)$], the dc-link current can be derived as [32]:

$$i_{Gdc}(s) = 1.5\frac{e_{Gd}(s)i_{Gd}(s)}{v_{DC}(s)} \tag{2}$$

Equation (2) can be linearized around the operating dc voltage V_{DC}, obtaining:

$$\tilde{i}_{Gdc}(s) = 1.5\frac{E_{Gd} + 2\,I_{Gd}\,R_{line} + I_{Gq}\,L_{line}\,\omega_1}{V_{DC}}\tilde{i}_{Gd}(s) \tag{3}$$

where E_{Gd}, I_{Gd} and I_{Gq} are the equilibrium values of $e_{Gd}(s)$, $i_{Gd}(s)$ and $i_{Gq}(s)$, respectively. Taking into account that the voltage drops at line resistance and inductance are small compared with the remaining term, equation (3) can be simplified as follows:

$$\tilde{i}_{Gdc}(s) = 1.5\frac{E_{Gd}}{V_{DC}}\tilde{i}_{Gd}(s) \tag{4}$$

On the other hand, it should be mentioned that the dynamics of inner current controllers are considered ideal: as the inner current loops are much faster than the outer loops, it is assumed that $i_{Gd}(t)$ and $i_{Gq}(t)$ references are followed instantaneously [33].

B. FESS

In this work, a FESS driven by an induction machine (IM) is employed, however the control strategy in this paper is also suitable for PMSM or BLDC driven FESS which have better performance in efficiency, power density and other aspects but

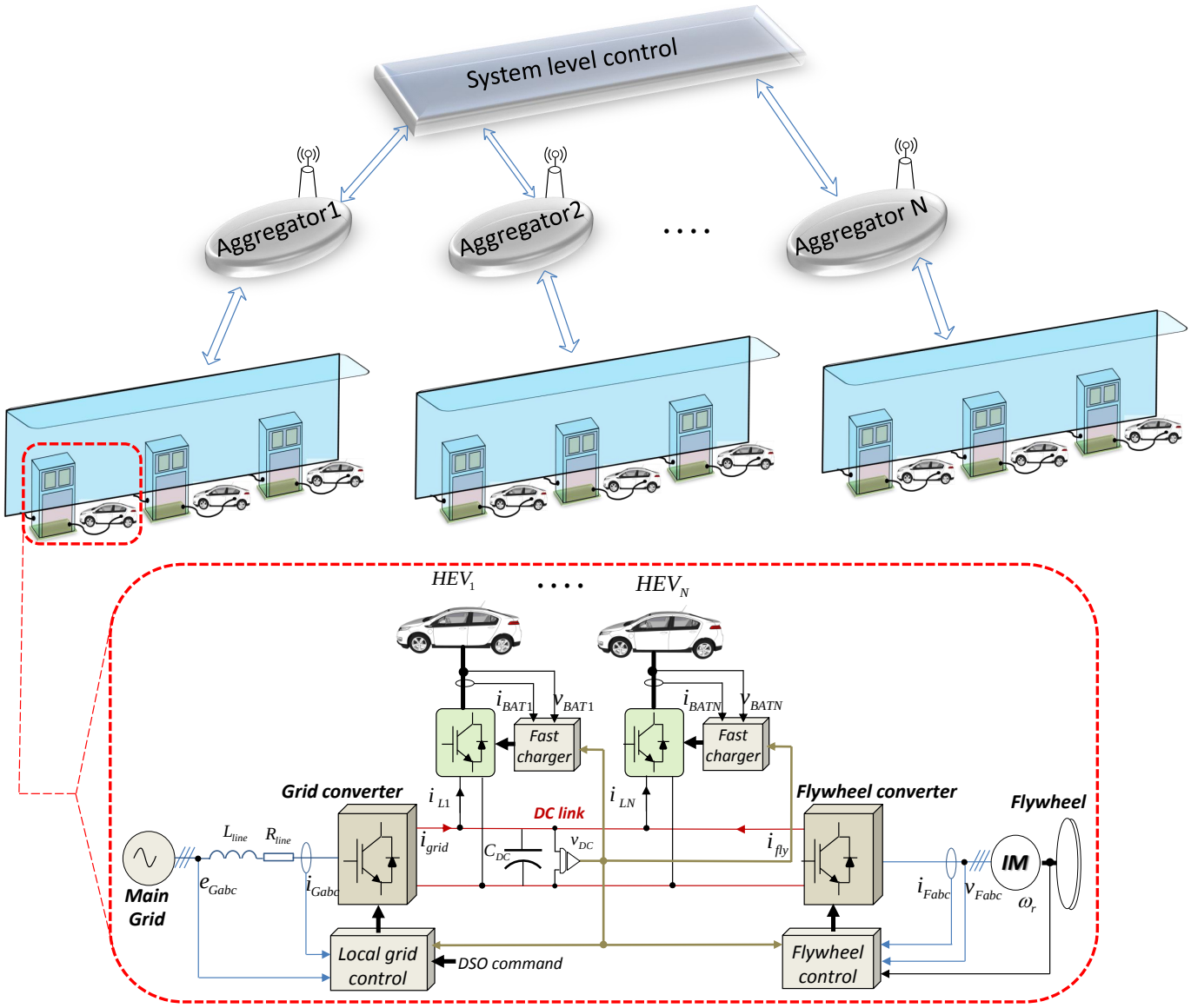

Fig. 1. Configuration of the FCS with dedicated FESS device and system level control structure.

with higher price [23]. Regarding control of induction machine, an indirect field oriented control (FOC) is considered. The rotor flux is aligned with the d-axis (i.e., $\psi_{rq}(t) = 0$), and hence its value is controlled by the d-axis current $i_{Fd}(t)$. Then, the q-axis component $i_{Fq}(t)$ controls the electric torque [25]. Since one of the FESS control objectives is to regulate the dc-link voltage, it is important to relate dc-link and q-axis currents [25]. The ac voltage equations at the converter terminals are given by:

$$\begin{aligned} v_{Fd}(t) =& R_s i_{Fd}(t) + \sigma L_s \frac{di_{Fd}(t)}{dt} - \omega_e \sigma L_s i_{Fq}(t) \\ v_{Fq}(t) =& R_s i_{Fq}(t) + \sigma L_s \frac{di_{Fq}(t)}{dt} + \omega_e \sigma L_s i_{Fd}(t) \\ &+ \omega_e \frac{L_0}{L_r} \psi_{rd}(t) \end{aligned} \tag{5}$$

where L_0 is the mutual inductance, L_s, L_r, R_s, R_r are stator and rotor inductances and resistances, respectively; ω_e is the flux rotational speed and σ is the total leakage coefficient [25]. From (5), its steady-state operation point can be well approximated by neglecting time-derivative terms, voltage drops in the resistances and slip [25], [34]. Under these assumptions, the steady-state voltages at the converter terminals are given by:

$$\begin{aligned} V_{Fd} &= 0 \\ V_{Fq} &= \omega_r L_0 I_{Fd} \end{aligned} \tag{6}$$

with ω_r being the mechanical speed.

The FESS current flowing towards the common dc bus can be expressed as:

$$i_{Fdc}(t) = 1.5 \frac{v_{Fd}(t) i_{Fd}(t) + v_{Fq}(t) i_{Fq}(t)}{v_{DC}(t)}. \tag{7}$$

Then, a small-signal model can be obtained by linearizing (7) around operating point defined by (6) and nominal dc-link voltage, giving rise to

$$\tilde{i}_{Fdc}(s) = 1.5\frac{\omega_r L_0 I_{Fd}}{V_{DC}}\tilde{i}_{Fq}(s) \tag{8}$$

with I_{Fd} being the equilibrium value of $i_{Fd}(s)$.

The swing equation of the FESS shows the changes in the rotational speed of the rotor

$$T_e(t) = J\frac{d\omega_r(t)}{dt} = 1.5\frac{p}{2}\frac{L_0^2}{L_r}I_{Fd}i_{Fq}(t), \tag{9}$$

where J is the FESS inertia and p is the number of pole pairs [34]. This expression is used to represent the mechanical dynamics and to tune the droop control loop responsible for DBS strategy.

C. PEV Battery

PEV battery is charged according to predefined charging profile recommended by manufacturer. This profile typically includes constant current charging stage followed by constant voltage charging stage [16]. Different from other works [12]–[14], the charging process of battery operates continuously without interruption and there is no discharging condition of battery either in this paper. The bandwidth of inner current and voltage control loops that regulate the charging process are normally in a Hz range and can be considered decoupled from other dynamics in the system [9]. Therefore, it can be concluded that the current introduced by the PEV load can be modeled as a disturbance, and it does not have an impact on dynamic properties of the system [9].

III. Implementation of FCS Control Strategy

This section explains the principal functionalities of hysteresis control strategy. Its main purpose is to interactively adjust the active power consumption of each singular FCS so that the aggregated loading of multiple FCSs behaves in a predefined way. It is foreseen that DSO regulates this aggregated characteristic by sending appropriate control signals to individual FCSs [14].

A. Tracking of DSO Commands

As shown in Fig. 2, DSO can shift the hysteresis characteristic up and down through the control signal $E_{DSO}(t)$. In that way, it can indirectly regulate the power consumption of FCS based on predicting variation of RES production and load consumption or other schemes [14], [35]. However, it should be noted that generation of $E_{DSO}(t)$ command is out of the scope of this paper. For that matter, the implementation of hysteresis control strategy is demonstrated here on a single FCS, while DSO signal is assumed to be predefined and is treated as an open loop input.

B. DBS for Coordinated Performance

It is well known that intermittent charging and termination of charging is undesirable for PEV battery, as it may cause the reduction of its lifetime [16]. Therefore, a dedicated FESS is used to achieve the hysteresis control objectives, but without compromising the recommended charging pattern of PEV battery. In order to integrate FESS within the FCS, coordination between FESS and grid converters needs to be established. It is important to highlight that this is achieved by a fully decentralized DBS control strategy [9]. The basic DBS principle is explained in the following paragraph.

Both grid and FESS converter are connected to a common dc bus. Therefore, a robust operation including continuous supply of PEV load, dc-link regulation and DSO average power tracking are mandatory control objectives. They are realized through the DBS strategy: the dc voltage reference includes a speed dependent droop controller.

$$\begin{aligned} T_e(s) =& (K_{pF} + \frac{K_{iF}}{s})\big[[V_{DCref} - V_{DC}(s)] \\ & - K_d[\omega_{mref} - \omega_r(s)]\big] \end{aligned} \tag{10}$$

with K_{pf} and K_{if} being constants of a PI controller, K_d is the droop constant.

The q-axis current reference $I_{Fqref}(s)$ is then obtained as follows [9]:

$$I_{Fqref}(s) = \frac{T_e(s)}{1.5\frac{p}{2}\frac{L_0^2}{L_r}I_{Fd}} \tag{11}$$

It should be noted that grid and FESS controllers adjust their operation by observing the deviation of dc bus voltage to realize the power balancing, and therefore, a digital communication between them is not needed [9]. It is also important to mention that, from a practical realization point of view, the maximum dc-link variations should be kept inside a safe operation range.

IV. System Modeling and Analysis

Fig. 2 shows the block diagram of an overall system controller. Besides the advanced techniques addressed in the previous section, it should be also bore in mind the non-linearities introduced in the controller. The effects of these non-linearities are detailed in this section.

First the full model of the system, as presented in Fig.2, was assembled in MATLAB/Simulink using the parameters in Table I. The dynamic response of dc voltage, speed of FESS and grid d-axis current are shown in Fig. 3a to 3c. From these figures, five operating modes can be identified (see also Table II).

- Mode I. Grid and FESS controllers are both activated. Dc-link voltage and speed of FESS are both at nominal value. Grid converter provides power for the loads and the losses in the system. FESS is in standby mode, meaning that it only extracts the power required to compensate its own losses.
- Mode II. Following the request from hysteresis controller to stop power extraction from grid converter, $i_{Gd}(t)$ is

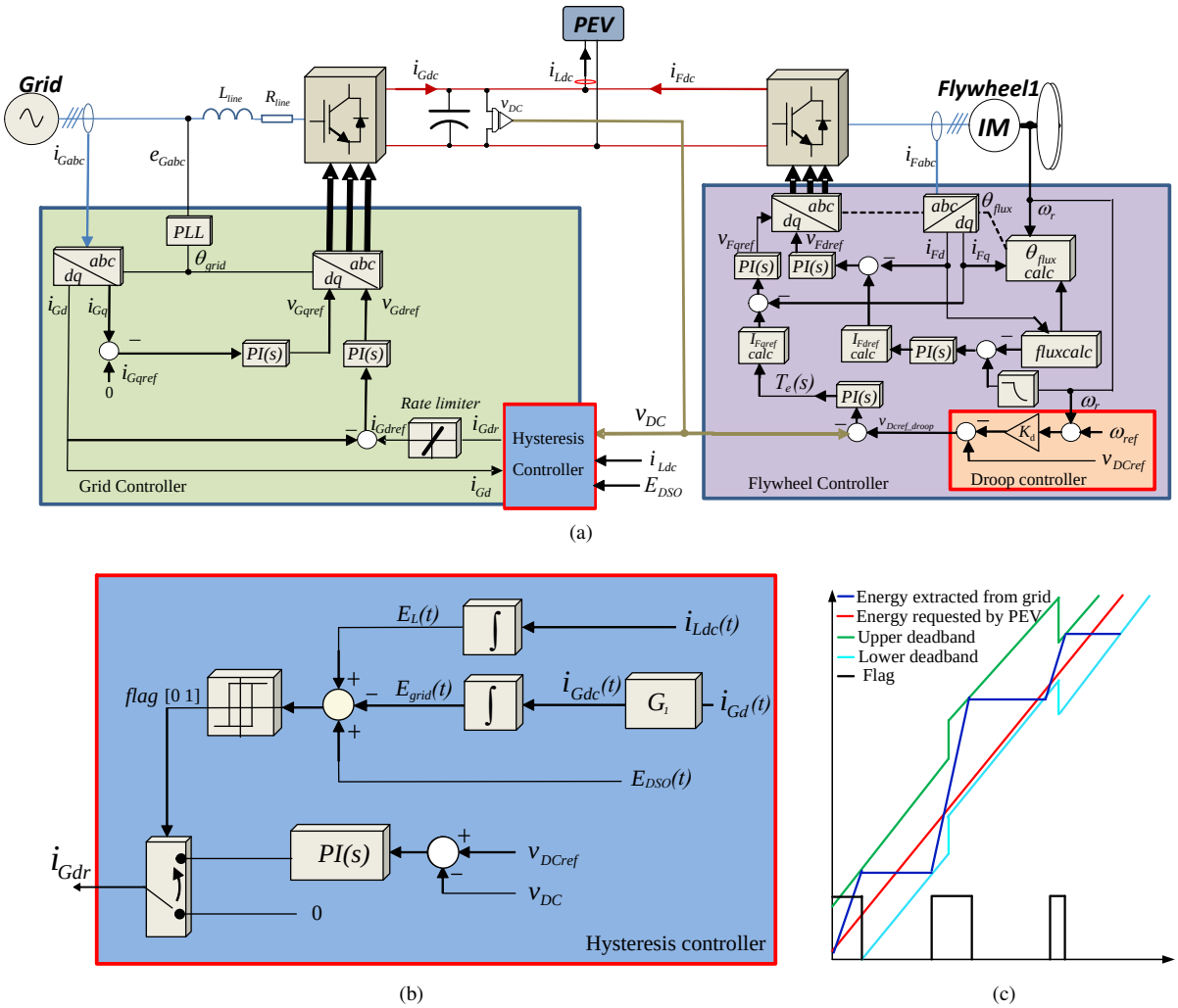

Fig. 2. Proposed FCS controller. (a) Overall control scheme. (b) Hysteresis controller. (c) Hystersis control signals.

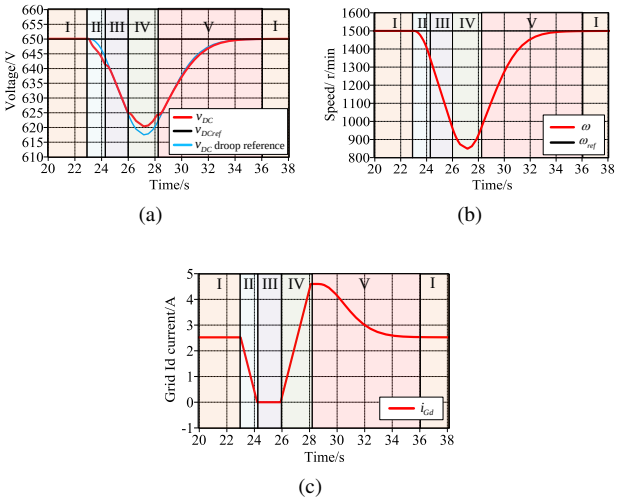

Fig. 3. Simulation results. (a) dc voltage. (b) Speed of FESS. (c) Grid d-axis current $i_{Gd}(t)$.

being ramped to zero due to saturation of rate limiter. The system can then be regarded as FESS with a ramping disturbance. Therefore, a minor error of dc bus voltage around 2.1 V can be seen in Fig. 3a. As shown later, the magnitude of this error can be limited by proper tuning of control parameters.

- Mode III. When $i_{Gd}(t)$ reaches zero value, only FESS is regulating the dc bus. Then, the dc voltage follows the reference imposed by droop control.
- Mode IV. Following the request from hysteresis controller to restart the grid converter, $i_{Gd}(t)$ is being ramped up towards a value set by a dc-link voltage controller. The dynamics of system is then equivalent to dynamics of Mode II.
- Mode V. The rate limiter gets unsaturated, and the grid and FESS controllers both regulate the dc bus. FESS is being recharged and its rotational speed is being recovered to nominal value. Correspondingly, dc voltage is also being restored back to its nominal value.

In the following, a more detailed description of each operating mode is provided.

TABLE I
ELECTRICAL AND CONTROL PARAMETERS

Electrical parameters		
dc-link capacitor	C_{DC}	2.2 mF
line inductance	L_{line}	3.8 mH
line resistance	R_{line}	0.2 Ω
dc resistive load	R_L	425 Ω
Grid voltage	V_{grid}	325 V
Induction machine parameters		
Stator inductance	L_s	301.0 mH
Rotor inductance	L_r	301.0 mH
Mutual inductance	L_0	289.4 mH
Stator resistance	R_s	1.945 Ω
Rotor resistance	R_r	2.3736 Ω
Total leakage coefficient	σ	0.0756
Pair of poles	p	2
Inertia	J	0.42 kgm^2
Grid controller parameters		
Proportional term	K_{pg}	0.3
Integral term	K_{ig}	0.12
slope of rate limiter	Δu	2 A/s
Sampling time	t_{s1}	1e-4 s
Flywheel controller parameters		
Proportional term	K_{pg}	0.35
Integral term	K_{ig}	3
Droop parameter	K_d	0.05
Sampling time	t_{s2}	1e-4 s

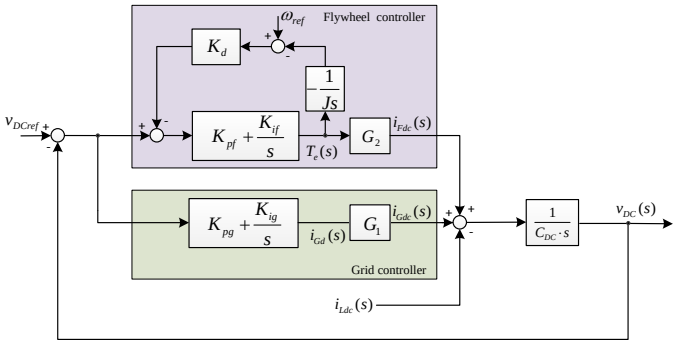

Fig. 4. Block diagram of grid and FESS.

A. Mode I: FESS Standby + Grid VSC

In Mode I, FESS and grid controllers are both activated. The FESS is in stand-by mode and operates at nominal speed. Grid converter is regulating the dc-link voltage by supplying the power for the PEV loads and losses of FESS.

By combining grid and FESS controllers, the small signal model shown in Fig. 4 can be obtained. In the block diagram, $G1$ is the gain from $i_{Gd}(s)$ to $i_{Gdc}(s)$, which was defined in (4) and is rewritten here for clarity:

$$G1 = 1.5\frac{E_{Gd}}{V_{DC}} \tag{12}$$

Accordingly, $G2$ is the gain from $T_e(s)$ to $i_{Fdc}(s)$, which is derived from (8) and (9), and can be expressed as:

$$G2 = \frac{2\omega_r L_r}{pL_0 V_{DC}} \tag{13}$$

The state space equation of the whole system can then be expressed as:

$$\begin{vmatrix} \dot{x_1} \\ \dot{x_2} \\ \dot{x_3} \\ \dot{x_4} \end{vmatrix} = \begin{vmatrix} 0 & K_{if}K_d & 0 & -K_{if} \\ -\frac{1}{J} & \frac{-K_{pf}K_d}{J} & 0 & 0 \\ 0 & 0 & 0 & -K_{ig} \\ \frac{G_2}{C_{DC}} & \frac{K_{pf}K_dG_2}{C_{DC}} & \frac{G_1}{C_{DC}} & -\frac{K_{pg}G_1+K_{pf}G_2}{C_{DC}} \end{vmatrix} \begin{vmatrix} x_1 \\ x_2 \\ x_3 \\ x_4 \end{vmatrix} + \begin{vmatrix} K_{if} & -K_{if}K_d & 0 \\ -\frac{-K_{pf}}{J} & \frac{K_{pf}K_d}{J} & 0 \\ K_{ig} & 0 & 0 \\ \frac{K_{pg}G_1+K_{pf}G_2}{C_{DC}} & \frac{K_{pf}K_dG_2}{C_{DC}} & \frac{1}{C_{DC}} \end{vmatrix} \begin{vmatrix} V_{DCref} \\ \omega_{ref} \\ i_{Ldc} \end{vmatrix} \tag{14}$$

where x_1, x_2, x_3 and x_4 are integrator output of FESS controller, speed of FESS, integrator output of grid controller and dc-link voltage, respectively.

Considering the parameters listed in Table I, following eigenvalues are obtained:

$$\begin{aligned} \lambda_1 &= -0.5\,\text{rad/s} \\ \lambda_2 &= -1.15 + i1.05\,\text{rad/s} \\ \lambda_3 &= -1.15 - i1.05\,\text{rad/s} \\ \lambda_4 &= -117.31\,\text{rad/s} \end{aligned} \tag{15}$$

This system is stable as all of its eigenvalues are in the left half plane. The slow eigenvalues $\lambda_1, \lambda_2, \lambda_3$ correspond to FESS inertia and droop control. On the other hand, λ_4 corresponds to the theoretical bandwidth of the dc-link voltage controller. In this mode, only λ_4 is excited since FESS is in stand-by.

B. Mode II: FESS Discharging with Ramping Disturbance

Mode II starts when the calculated actual energy $E_{grid}(t)$, which is obtained by integral of the grid dc current $i_{Gdc}(t)$, intersects with the upper dead-band. The hysteresis controller switches its output to zero and saturates the rate limiter, and hence the current $i_{Gd}(t)$ decreases in a ramping manner due to the saturation. This causes a dip in dc-link voltage, which leads the FESS to supply the load power. Consequently, FESS decreases its rotational speed.

In this mode, the system can be analyzed as an FESS with a ramping disturbance from grid controller. The corresponding control block diagram is showed in Fig. 5. The corresponding state space equation is expressed as follows:

$$\begin{vmatrix} \dot{x_1} \\ \dot{x_2} \\ \dot{x_4} \end{vmatrix} = \begin{vmatrix} 0 & K_{if}K_d & -K_{if} \\ -\frac{1}{J} & \frac{-K_{pf}K_d}{J} & 0 \\ \frac{G_2}{C_{DC}} & \frac{K_{pf}K_dG_2}{C_{DC}} & -\frac{K_{pf}G_2}{C_{DC}} \end{vmatrix} \begin{vmatrix} x_1 \\ x_2 \\ x_4 \end{vmatrix} + \begin{vmatrix} K_{if} & -K_{if}K_d & 0 \\ -\frac{-K_{pf}}{J} & \frac{K_{pf}K_d}{J} & 0 \\ \frac{K_{pf}G_2}{C_{DC}} & \frac{K_{pf}K_dG_2}{C_{DC}} & \frac{1}{C_{DC}} \end{vmatrix} \begin{vmatrix} V_{DCref} \\ \omega_{ref} \\ i_{Ldc} \end{vmatrix} \tag{16}$$

where the x_1, x_2 and x_4 are the same as in operating Mode I. Using the parameters listed in Table I, the following eigenvalues are obtained:

$$\begin{aligned} \lambda_1 &= -0.5\,\text{rad/s} \\ \lambda_2 &= -15.11 + i5.84\,\text{rad/s} \\ \lambda_3 &= -15.11 - i5.84\,\text{rad/s} \end{aligned} \tag{17}$$

TABLE II
OPERATION SECTIONS IN ONE CYCLE OF SYSTEM

Operation mode	System model	dc voltage	FESS condition
I	FESS + Grid VSC	Nominal value	Standby at nominal speed
II	FESS + Ramping disturbance	Error	Discharging
III	Only FESS	Droop reference	Discharging
IV	FESS + Ramping disturbance	Error	Discharging to charging
V	FESS + Grid VSC	Droop reference	Charging

The system has one dominant real negative eigenvalue and two eigenvalues with real negative and imaginary parts, and consequently it has a stable under damped response. The eigenvalue $\lambda_1 = -0.5\,\mathrm{rad/s}$ corresponds to the FESS inertia and determines the system's dominant time constant of $2\,\mathrm{s}$.

The error in the dc-link voltage during the ramping disturbance can be expressed in (18). According to the final value theorem, when there is a ramping disturbance $\frac{\Delta u}{s^2}$, the dc voltage error is given by (19).

This means that there is an error between dc voltage and dc droop reference when rate limiter is acting. However, the ramping periods are short (around $1\,\mathrm{s}$) and the error can be controlled within specified limits. As C_{DC} is much smaller than other terms, the most influential is K_{if}. With the parameters in Table I, the error is around $2\,\mathrm{V}$, which is acceptable. The grid benefits from ramping behavior to avoid sudden power stress at the expense of small tracking error.

C. Mode III: Only FESS

Mode III begins at the point when the current $i_{Gd}(t)$ reaches zero and the FESS provides all the power to load. The dc bus voltage is regulated according to the droop law defined by (10). The dc current from grid $i_{Gdc}(t)$ is zero. The corresponding control diagram is shown in Fig. 6.

The system in this mode has the same state equation and eigenvalues as in the Mode II but without ramping disturbance, hence the steady state error in dc-link voltage is zero. The system operates with the time constant of $2\,\mathrm{s}$ which is associated with eigenvalue $-0.5\,\mathrm{rad/s}$.

According to the droop law (10), droop parameter K_d directly determines the dc-link voltage variation. In order to study its influence, the dominant eigenvalues are shown in Fig. 7 when K_d changes from 0.01 to 0.2 with a step of 0.01. It is observed that, if K_d is too small, the dominant eigenvalue is closer to imaginary axis which can jeopardize the stability of system. If K_d is too big, it may cause big variation of dc-link voltage. Hence, K_d is chosen as 0.05 as a trade-off: This value causes maximum dc voltage variation around $30\,\mathrm{V}$, which is acceptable [36], [37].

D. Mode IV: FESS Charging with Ramping Disturbance

The system switches to Mode IV when the calculated actual energy reaches the lower dead-band. Then the $i_{Gd}(t)$ reference of grid controller starts to be generated by a dc-link voltage PI controller, even though its output is ramp limited. At certain point, when the grid current equalizes with and exceeds the load current, the FESS stops discharging and its rotational speed begins to increase, causing the dc-link bus to recover back.

The dynamic characteristic in this mode is exactly the same as Mode II and there also exists an error of around $2\,\mathrm{V}$ between dc-link voltage and droop reference.

E. Mode V: FESS Charging + Grid VSC

The system moves to operating Mode V when the rate limiter gets deactivated. Therefore, the system presents the same dynamics as in Mode I. However, the practical difference is in a fact that FESS is not in standby mode, but is being recharged. Therefore, it is possible to identify the slow eigenvalues in the response of the system. After the FESS reaches its nominal speed, the system is switched back to Mode I and the full cycle of operation is completed.

V. EXPERIMENTAL RESULTS

In order to test the feasibility of the theoretical analysis done, a downscaled experimental setup was builtwith the parameters described in Table I in Microgird lab in Aalborg university. Fig. 8 shows the experimental setup consisting of two Danfoss $2.2\,\mathrm{kW}$ inverters, a FESS driven by a $2.2\,\mathrm{kW}$ induction machine, voltage and current LEM sensors, input L filter, and dSPACE1006 to implement the proposed control algorithm. The switching frequency of the inverters was set to $10\,\mathrm{kHz}$. The system was connected to the grid through a $10\,\mathrm{kVA}$ isolation transformer, and a resistive load was used to emulate PEV loads [38]. In order to demonstrate the performance of the system in reduced time, the experiment was performed in seconds timescale.

A. Hysteresis Charging without DSO Command Signals

Fig. 9 represents the experimental results in one hysteresis cycle. First, the system is operating at Mode I where dc bus voltage is $650\,\mathrm{V}$ and the speed of FESS is at nominal speed $1500\,\mathrm{rpm}$. Around $3\,\mathrm{s}$, the hysteresis control signal in Fig. 9d intersects the upper band limit, hence the grid current starts to decrease to zero, causing the drop of dc bus voltage. At the same time, FESS reduces its rotational speed and compensates the active power of the load. During the ramping periods, there exists an error around $2\,\mathrm{V}$ between dc bus voltage and the reference set by droop.

After the $i_{Gd}(t)$ reaches zero, only FESS regulates the dc bus and the dc voltage tracks the droop reference precisely. At $6\,\mathrm{s}$, the hysteresis control signal reaches the lower band limit and the FESS reaches its lowest speed. Also, the dc bus voltage drops to a minimum value of around $620\,\mathrm{V}$ according to the chosen value of K_d. Then the grid converter starts to

$$E_v(s) = i_{Gdc}(s)\frac{Js}{JC_{DC}s^2 + (C_{DC}K_dK_{pf} + G_2JK_{pf})s + K_dK_{if}C_{DC} + K_{if}G_2J} \tag{18}$$

$$\begin{aligned} E_v|_{t\longrightarrow\infty} &= \lim_{s\longrightarrow 0} sE_v(s) \\ &= \lim_{s\longrightarrow 0} s\frac{\Delta u}{s^2}\frac{Js}{JC_{DC}s^2 + (C_{DC}K_dK_{pf} + G_2JK_{pf})s + K_dK_{if}C_{DC} + K_{if}G_2J} \\ &= \frac{J}{K_dK_{if}C_{DC} + K_{if}G_2J} \end{aligned} \tag{19}$$

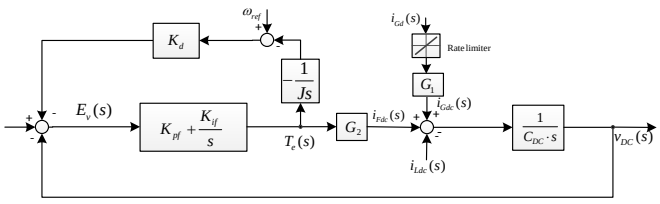

Fig. 5. Block diagram of FESS with ramping disturbance.

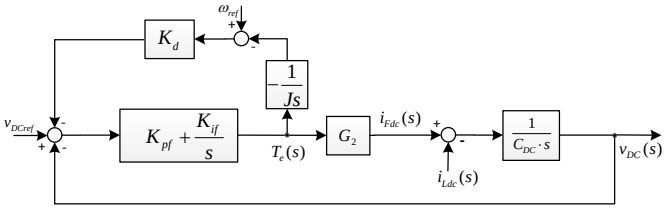

Fig. 6. Block diagram of mode when only FESS is active.

be controlled by a PI controller, while the rate limiter gets saturated again due to the dc bus voltage deviation. Therefore, a small error of dc voltage appears again until around $8.5\,\mathrm{s}$ when the rate limiter runs out of saturation zone.

Finally, around $18\,\mathrm{s}$, the dc voltage and the FESS speed reach their respective nominal values. One may observe that the FESS dc current is not zero when the FESS has recharged to nominal speed, which is caused by friction and electromagnetic losses. Experiments are carried out when the

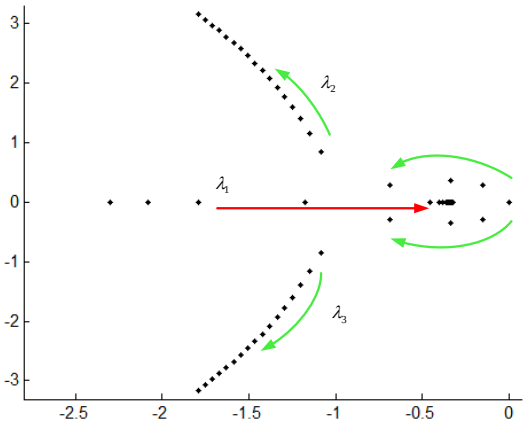

Fig. 7. Dominant eigenvalues as a function of K_d from 0.01 to 0.2.

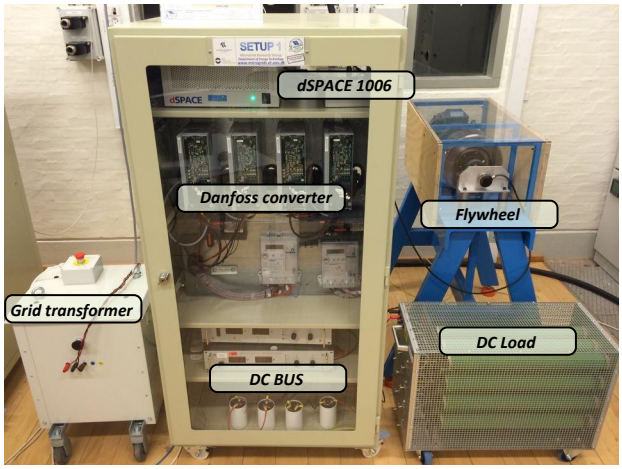

Fig. 8. Laboratory prototype.

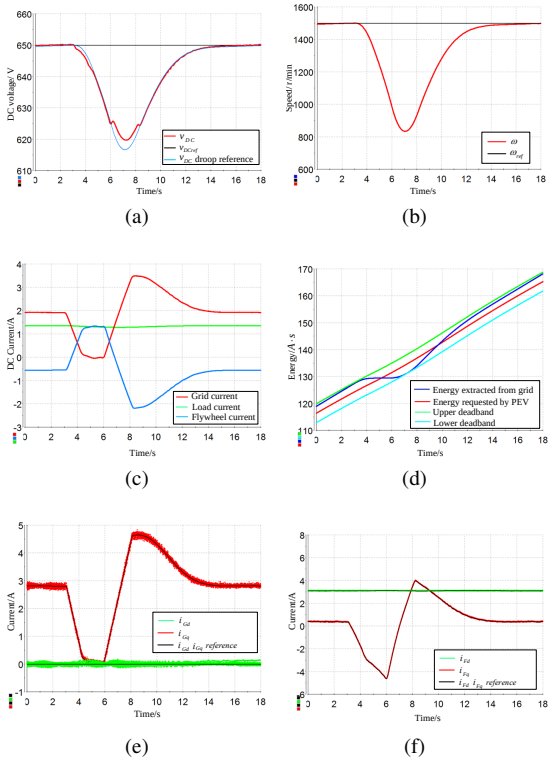

Fig. 9. Experimental results when FESS runs low speed region: below base speed $<$ 1500 rpm. (a)dc voltage. (b) Speed of FESS. (c) dc current. (d) Hysteresis control signals without DSO reference. (e) $i_{Gd}(t)$, $i_{Gq}(t)$ and reference. (f) $i_{Fd}(t)$, $i_{Fq}(t)$ and reference.

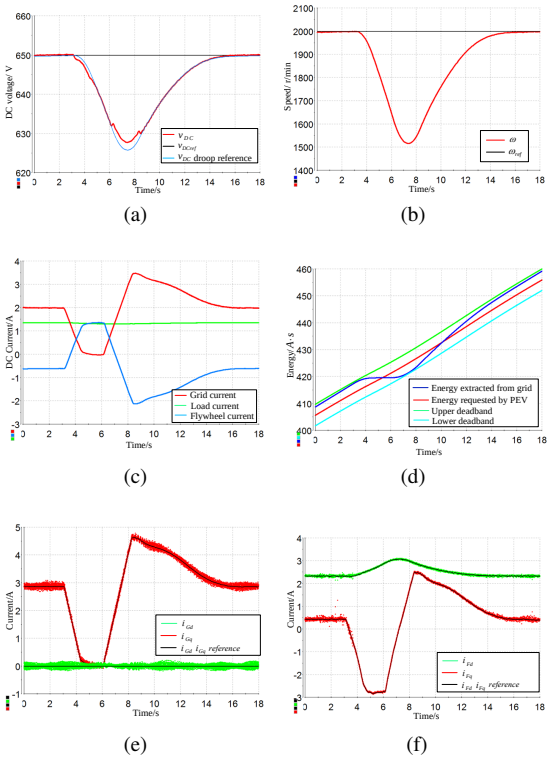

(a) (b) (c) (d) (e) (f)

Fig. 10. Experimental results when FESS runs at high speed region: over base speed $1500 - 2000\,\mathrm{rpm}$. (a)dc voltage. (b) Speed of FESS. (c) dc current. (d) Hysteresis control signals without DSO reference. (e) $i_{Gd}(t)$, $i_{Gq}(t)$ and reference. (f) $i_{Fd}(t)$, $i_{Fq}(t)$ and reference.

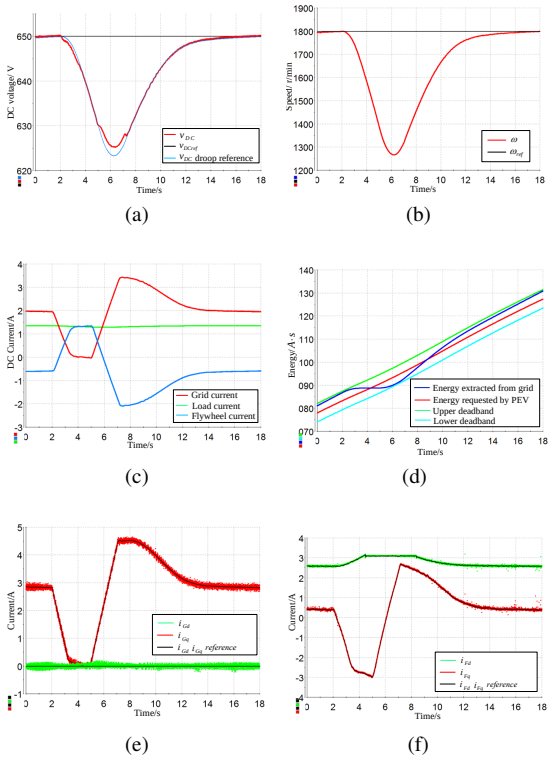

(a) (b) (c) (d) (e) (f)

Fig. 11. Experimental results when FESS runs at medium speed region: $1200 - 1800\,\mathrm{rpm}$. (a)dc voltage. (b) Speed of FESS. (c) dc current. (d) Hysteresis control signals without DSO reference. (e) $i_{Gd}(t)$, $i_{Gq}(t)$ and reference. (f) $i_{Fd}(t)$, $i_{Fq}(t)$ and reference.

FESS is operating at high speed and medium speed region. The respective results are presented in Fig. 10 and Fig. 11, respectively. One may observe that the current of FESS $i_{Fd}(t)$ decreases due to the field weakening when the speed is over base speed. The results show that in each region the system can adjust its operation and manage to automatically implement smooth charging and discharging.

B. System Response with DSO Commands

According to the control diagram, the command signals from DSO can shift the band limits up and down to regulate the grid energy consumption [35]. As shown in Fig. 12, the system is charging according to nominal hysteresis control scheme until $28\,\mathrm{s}$ when DSO sends a signal +2, causing the band limit shifting up. Hence the grid controller stays on-state until the calculated energy consumption reaches the updated upper band limit. As a result, the energy consumption increases. Accordingly, at around $48\,\mathrm{s}$, DSO sends a signal -2, leading to the band limit shifting down, and then the grid controller transfers to off-state earlier, which means the load consumption decreases.

C. System Response when the Grid Power is Lost

As is shown in Fig. 13, when the the grid power is lost, grid current steps to zero and causes a dip of dc bus voltage. Then the FESS takes charge of dc bus regulation with fast response, and supplies all the active power for the load by decreasing its speed, and the dc bus changes according to the droop law.

D. System Response when the Load is Disconnected

As is shown in Fig. 14, when the load is disconnected suddenly around $2\,\mathrm{s}$, load current steps to zero and causes a increase of dc bus voltage in the transient. Then the dc current of grid converter will decrease but limited by rate limiter, which causes the FESS to increase its speed to absorb the power from grid converter, and the dc bus voltage is regulated according to the droop law with the change of speed. At the point when grid current equalizes with the current caused by FESS losses, the FESS starts to decrease its speed. Finally the FESS reaches its nominal speed, the dc bus also returns back to the nominal value and grid converter supplies the active power for FESS losses and regulates the dc bus.

VI. Conclusion

This paper carried out theoretical and experimental validation of a hysteresis-type active power support scheme from a FCS equipped with FESS. The control strategy employs a droop-based DBS control method to avoid digital communication between grid and FESS converters. The proposed algorithm provides a good response to system-level signals from DSO while not interrupting the predefined charging profiles of PEV battery. In order to analyze the characteristics

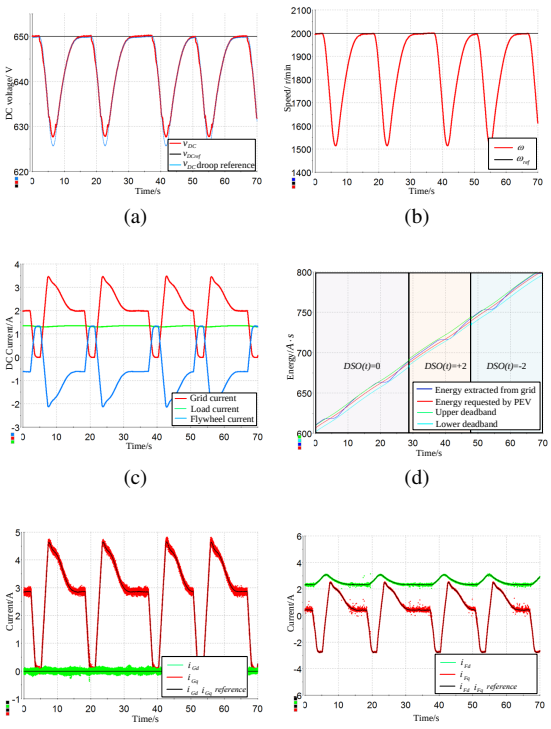

(a) (b) (c) (d) (e) (f)

Fig. 12. Experimental results of system response following DSO command. (a)dc voltage. (b) Speed of FESS. (c) dc current. (d) Hysteresis control signals with DSO reference. (e) $i_{Gd}(t)$, $i_{Gq}(t)$ and reference. (f) $i_{Fd}(t)$, $i_{Fq}(t)$ and reference.

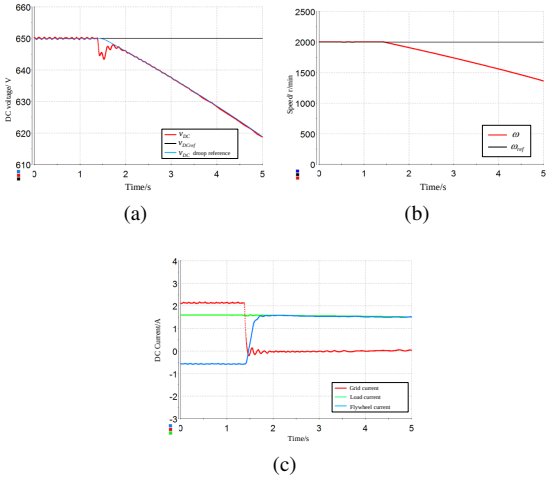

(a) (b) (c)

Fig. 13. Experimental results of system response when the grid is lost. (a) dc voltage. (b) Speed of FESS. (c) dc current.

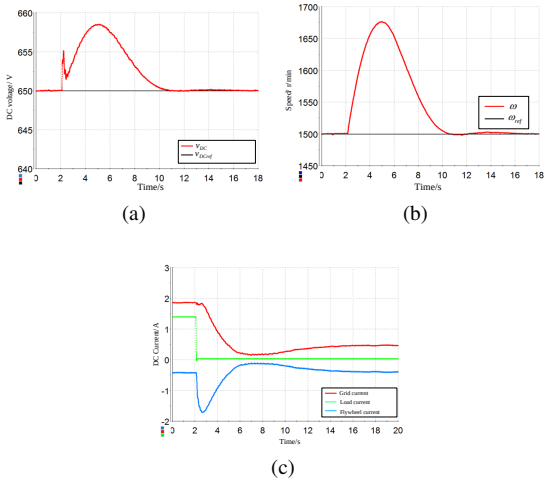

(a) (b) (c)

Fig. 14. Experimental results of system response when the load is disconnected. (a) dc voltage. (b) Speed of FESS. (c) dc current.

of the system, a small signal model has been assembled to explain its dynamics in each operating mode. It is shown that the grid and FESS controllers realize the power balancing and compensation in a coordinated and stable manner. Finally, experimental results on a reduced scale lab prototype have been presented to verify the feasibility of this control method.

REFERENCES

[1] Z. Chen, J. Guerrero, and F. Blaabjerg, "A review of the state of the art of power electronics for wind turbines," *IEEE Trans. Power Electron.*, vol. 24, no. 8, pp. 1859–1875, 2009.

[2] L. Nousiainen, J. Puukko, A. Maki, T. Messo, and J. Huusari, "Photovoltaic generator as an input source for power electronic converters," *IEEE Trans. Power Electron.*, vol. 28, no. 6, pp. 3028–3038, 2013.

[3] J. Guerrero, J. Vasquez, J. Matas, L. D. Vicu, and M. Castilla, "Hierarchical control of droop-controlled AC and DC microgrids—a general approach toward standardization," *IEEE Trans. Power Electron.*, vol. 58, no. 1, pp. 158–172, 2011.

[4] F.Blaabjerg, R. Teodorescu, and M. Liserre, "Overview of control and grid synchronization for distributed power generation systems," *IEEE Trans. Ind. Electron.*, vol. 53, no. 5, pp. 1398–1409, 2006.

[5] G. Strbac, "Demand side management: Benefits and challenges," *Energy policy*, vol. 36, no. 12, pp. 4419–4426, 2008.

[6] M. Klobasa, "Analysis of demand response and wind integration in Germany's electricity market," *IET Renewable Power Generat.*, vol. 4, no. 1, pp. 55–63, 2010.

[7] K. Clement-Nyns, E. Haesen, and J. Driesen, "The impact of charging plug-in hybrid electric vehicles on a residential distribution grid," *IEEE Trans. Power Syst.*, vol. 25, no. 1, pp. 371–380, 2010.

[8] M. Yilmaz and P. Krein, "Review of battery charger topologies, charging power levels, and infrastructure for plug-in electric and hybrid vehicles," *IEEE Trans. Power Electron.*, vol. 28, no. 5, pp. 2151–2169, 2013.

[9] T. Dragicevic, S. Sucic, J. C. Vasquez, and J. Guerrero, "Flywheel-based distributed bus signalling strategy for the public fast charging station," *IEEE Trans. Smart Grid*, vol. 5, no. 6, pp. 2825–2835, 2014.

[10] S. Bai and S. Lukic, "Unified active filter and energy storage system for an mw electric vehicle charging station," *IEEE Trans. Power Electron.*, vol. 28, no. 12, pp. 5793–5803, 2013.

[11] D. Dallinger, J. Link, and M. Btner, "Smart grid agent: Plug-in electric vehicle," *IEEE Trans. Sustain. Energy.*, vol. 5, no. 3, pp. 710–717, 2014.

[12] E. Sortomme and K. Cheung, "Intelligent dispatch of electric vehicles performing vehicle-to-grid regulation," in *IEEE International Electric Vehicle Conference (IEVC) 2012, Greenville, SC, USA*, 2012.

[13] M. D. Galus, S. Koch, and G. Andersson, "Provision of load frequency control by phevs, controllable loads, and a cogeneration unit," *IEEE Trans. Ind. Electron.*, vol. 58, no. 10, pp. 4568–4582, 2011.

[14] D. Callaway and I. Hiskens, "Achieving controllability of electric loads," *Proc. IEEE*, vol. 99, no. 1, pp. 184–199, 2011.

[15] D. Callaway, "Tapping the energy storage potential in electric loads to deliver load following and regulation, with application to wind energy," *Energy Conversion and Management*, vol. 50, no. 5, pp. 1389–1400, 2009.

[16] D. Linden and T. B. Reddy, *Handbook of batteries*. McGraw-Hill, 2002.

[17] S. Vazquez, S. Lukic, E. Galvan, L. Franquelo, and J. Carrasco, "Energy storage systems for transport and grid applications," *IEEE Trans. Ind. Electron.*, vol. 57, no. 12, pp. 3881–3895, 2010.

[18] A. Oudalov, D. Chartouni, and C. Ohler, "Optimizing a battery energy storage system for primary frequency control," *IEEE Trans. Power Syst.*, vol. 22, no. 3, pp. 1259–1266, 2007.

[19] J. Barton and D. Infield, "Energy storage and its use with intermittent renewable energy," *IEEE Trans. Energy Convers.*, vol. 19, no. 2, pp. 441–448, 2004.

[20] G. Cimuca, S. Breban, M. Radulescu, C. Saudemont, and B. Robyns, "Design and control strategies of an induction-machine-based flywheel energy storage system associated to a variable-speed wind generator," *IEEE Trans. Energy Convers.*, vol. 25, no. 2, pp. 526–534, 2010.

[21] M. Poloujadoff, C. Rioux, and M. M. Radulescu, "On the flywheel design for energy storage systems," *Electromotion*, vol. 13, no. 4, pp. 271–275, 2006.

[22] V. Babuska, S. Beatty, B. deBlonk, and J. Fausz, "A review of technology developments in flywheel attitude control and energy transmission systems," in *Aerospace Conference, 2004. Proceedings. 2004 IEEE*, vol. 4, 2004, pp. 2784–2800.

[23] M. Awadallah and B. Venkatesh, "Energy storage in flywheels: An overview," *Canadian Journal of Electric. and Comput. Engineering.*, vol. 38, no. 2, pp. 183–193, 2015.

[24] H. Akagi and H. Sato, "Control and performance of a doubly-fed induction machine intended for a flywheel energy storage system," *IEEE Trans. Power Electron.*, vol. 17, no. 1, pp. 109–116, 2002.

[25] R. Cardenas, R. Pena, G. Asher, J. Clare, and R. Blasco-Gimenez, "Control strategies for power smoothing using a flywheel driven by a sensorless vector-controlled induction machine operating in a wide speed range," *IEEE Trans. Ind. Electron.*, vol. 51, no. 3, pp. 603–614, 2004.

[26] S. Samineni, B. Johnson, H. Hess, and J. Law, "Modeling and analysis of a flywheel energy storage system for voltage sag correction," *IEEE Trans. Industry Appl.*, vol. 42, no. 1, pp. 42–52, 2006.

[27] G. Cimuca, C. Saudemont, B. Robyns, and M. Radulescu, "Control and performance evaluation of a flywheel energy-storage system associated to a variable-speed wind generator," *IEEE Trans. Ind. Electron.*, vol. 53, no. 4, pp. 1074–1085, 2006.

[28] X. Chang, Y. Li, W. Zhang, N. Wang, and W. Xue, "Active disturbance rejection control for a flywheel energy storage system," *IEEE Trans. Ind. Electron.*, vol. 62, no. 2, pp. 991–1001, 2015.

[29] J. Schonberger, R. Duke, and S. Round, "DC-bus signaling: A distributed control strategy for a hybrid renewable nanogrid," *IEEE Trans. Ind. Electron.*, vol. 53, no. 5, pp. 1453–1460, 2006.

[30] K. Sun, L. Zhang, Y. Xing, and J. M. Guerrero, "A distributed control strategy based on DC bus signaling for modular photovoltaic generation systems with battery energy storage," *IEEE Trans. Power Electron.*, vol. 26, no. 10, pp. 3032–3045, 2011.

[31] T. Dragicevic, J. Guerrero, J. Vasquez, and D. Skrlec, "Supervisory control of an adaptive-droop regulated DC microgrid with battery management capability," *IEEE Trans. Power Electron.*, vol. 29, no. 2, pp. 695–706, 2014.

[32] V. Blasko and V. Kaura, "A new mathematical model and control of a three-phase AC-DC voltage source converter," *IEEE Trans. Power Electron.*, vol. 12, no. 1, pp. 116–123, 1997.

[33] A. Vidal, A. Yepes, F. Freijedo, J. Malvar, O. Lopez, and J. Doval-Gandoy, "A technique to estimate the equivalent loss resistance of grid-tied converters for current control analysis and design," *IEEE Trans. Power Electron.*, vol. 30, no. 3, pp. 1747–1761, 2015.

[34] D. W. Novotny and T. A. Lipo, *Vector Control and Dynamics of AC Drives*. OXFORD, 1996.

[35] T. Dragicevic, B. Sun, E. Schaltz, and J. Guerrero, "Flexible local load controller for fast electric vehicle charging station supplemented with flywheel energy storage system," in *IEEE International Electric Vehicle Conference (IEVC) 2014, Florence, Italy*, 2014.

[36] D. Wu, F. Tang, T. Dragicevic, J. Guerrero, and J. Vasquez, "Coordinated control based on bus-signaling and virtual inertia for islanded DC microgrids," *IEEE Trans. Smart Grid*, 2015.

[37] *IEEE Recommended Practice for Emergency and Standby Power Systems for Industrial and Commercial Applications*, IEEE Standard Std., 1995.

[38] S. Rivera, W. Bin, S. Kouro, V. Yaramasu, and W. Jiacheng, "Electric vehicle charging station using a neutral point clamped converter with bipolar dc bus," *IEEE Trans. Ind. Electron.*, vol. 62, no. 4, pp. 1999–2009, 2015.

Bo Sun received the B.S. and M.S. degrees in electrical engineering from Harbin Institute of Technology, Harbin, China, in 2011 and 2013, respectively. He is currently working toward the Ph.D. degree in the Department of Energy Technology, Aalborg University, Aalborg, Denmark.

His research interests include power electronics, modeling, control, and energy management of distributed power systems based on renewable energy sources and energy storage technologies.

Tomislav Dragicevic (S09-M13) received the M.E.E. and the industrial Ph.D. degree from the Faculty of Electrical Engineering, Zagreb, Croatia, in 2009 and 2013, respectively. His PhD thesis has been carried out in close cooperation with industry and he has received highest honors for it. He is currently a research associate at the Institute of Energy Technology, Aalborg University. His principal field of interest is overall system design of autonomous and grid connected DC and AC microgrids, and industrial application of advanced modelling, control and protection concepts to shipboard power systems, remote telecom stations, domestic and commercial facilities and electric vehicle charging stations. He has authored and co-authored more than 60 technical papers in his domain of interest. 20 of them are published in international journals. Dr. Dragievi is a Member of the IEEE Power Electronics and IEEE Power Systems Societies. He has served in Scientific Committee Boards in several IEEE conferences and has been invited for guest lectures and tutorials in universities and companies around the world.

Francisco D. Freijedo received the M.Sc. degree in Physics from the University of Santiago de Compostela, Santiago de Compostela, Spain, in 2002 and the Ph.D. degree from the University of Vigo, Vigo, Spain, in 2009.

From 2005 to 2011, he was a Lecturer with the Department of Electronics Technology of the University of Vigo. From 2011 to 2014, he worked in the wind power industry as a control engineer.

Since 2014, he is a Postdoctoral Researcher at the Department of Energy Technology of Aalborg University. His main research interests are in the areas of ac power conversion.

Juan C. Vasquez (M12-SM14) received the B.S. degree in Electronics Engineering from the Autonomous University of Manizales, Manizales, Colombia, and the Ph.D. degree in Automatic Control, Robotics, and Computer Vision from the Technical University of Catalonia, Barcelona, Spain, in 2004 and 2009, respectively. He was with the Autonomous University of Manizales working as a teaching assistant and the Technical University of Catalonia as a Post-Doctoral Assistant in 2005 and 2008 respectively. In 2011, he was Assistant Professor and from 2014 he is working as an Associate Professor at the Department of Energy Technology, Aalborg University, Denmark where he is the Vice Programme Leader of the Microgrids Research Program. From Feb. 2015 to April. 2015 he was a Visiting Scholar at the Center of Power Electronics Systems (CPES) at Virginia Tech. His current research interests include operation, advanced hierarchical and cooperative control, optimization and energy management applied to distributed generation in AC and DC microgrids. He has authored and co-authored more than 100 technical papers only in Microgrids where 60 of them are published in international IEEE journals.

Dr. Vasquez is currently a member of the IEC System Evaluation Group SEG4 on LVDC Distribution and Safety for use in Developed and Developing Economies, the Renewable Energy Systems Technical Committee TC-RES in IEEE Industrial Electronics, PELS, IAS, and PES Societies.

Josep M. Guerrero (S01-M04-SM08-FM15) received the B.S. degree in telecommunications engineering, the M.S. degree in electronics engineering, and the Ph.D. degree in power electronics from the Technical University of Catalonia, Barcelona, in 1997, 2000 and 2003, respectively. Since 2011, he has been a Full Professor with the Department of Energy Technology, Aalborg University, Denmark, where he is responsible for the Microgrid Research Program. From 2012 he is a guest Professor at the Chinese Academy of Science and the Nanjing University of Aeronautics and Astronautics; from 2014 he is chair Professor in Shandong University; and from 2015 he is a distinguished guest Professor in Hunan University.

His research interests is oriented to different microgrid aspects, including power electronics, distributed energy-storage systems, hierarchical and cooperative control, energy management systems, and optimization of microgrids and islanded minigrids. Prof. Guerrero is an Associate Editor for the IEEE TRANSACTIONS ON POWER ELECTRONICS, the IEEE TRANSACTIONS ON INDUSTRIAL ELECTRONICS, and the IEEE Industrial Electronics Magazine, and an Editor for the IEEE TRANSACTIONS on SMART GRID and IEEE TRANSACTIONS on ENERGY CONVERSION. He has been Guest Editor of the IEEE TRANSACTIONS ON POWER ELECTRONICS Special Issues: Power Electronics for Wind Energy Conversion and Power Electronics for Microgrids; the IEEE TRANSACTIONS ON INDUSTRIAL ELECTRONICS Special Sections: Uninterruptible Power Supplies systems, Renewable Energy Systems, Distributed Generation and Microgrids, and Industrial Applications and Implementation Issues of the Kalman Filter; and the IEEE TRANSACTIONS on SMART GRID Special Issue on Smart DC Distribution Systems. He was the chair of the Renewable Energy Systems Technical Committee of the IEEE Industrial Electronics Society. He received the 2014 best paper award of the IEEE Transactions on Energy Conversion. In 2014 and 2015 he was awarded by Thomson Reuters as Highly Cited Researcher, and in 2015 he was elevated as IEEE Fellow for his contributions on distributed power systems and microgrids.